Theoretical analysis of the output noise of a DFB fiber laser sensor

Dan Savastru, Sorin Miclos, and Ion Lancranjan

***Abstract*—** The results of a theoretical analysis of the output noise generated by the DFB fiber laser sensor with applications mainly in the field of the aeronautical applications are presented. The main purpose of this analysis is to evaluate the magnitude of the DFB fiber laser sensor output noise. This evaluation is necessary for a proper design of the sensor, especially regarding sensitivity and dynamic range. It is demonstrated that the main source of DFB fiber laser sensor output noise is constituted by the Amplified Spontaneous Emission (ASE) of the fiber amplifier. An extended range of linear response was achieved optimizing the sensor parameters. ASE noise level was brought to an acceptable level. Judging the time response, the designed sensor acts like a high fidelity recorder.

***Keywords*—**DFB fiber laser sensor, ASE, fiber amplifier, sensor

I. Introduction

THIS paper is a theoretical attempt relying on numerical simulations when necessary performed in order to get some insight on using a new and promising class of sensors for aeronautical applications, namely active Fiber Bragg Grating (FBG) known also as Distributed Feed Back Fiber Laser (DFB-FL).

Distributed feedback fiber lasers (DFB-FL) and distributed Bragg reflector fiber lasers (DBR-FL) possess certain unique properties that make them quite attractive for a number of different applications. They are inherently fiber compatible, and very simple passive thermal stabilization is sufficient to ensure the stability of the laser. A number of different active dopants, such as erbium, ytterbium, neodymium, and thulium, can be used in order to cover different windows of the optical spectrum. These features, combined with the ability to define the emitted wavelength precisely through the grating structure along with the narrow linewidth and low relative intensity noise (RIN), make DFB-FL and DBR-FL very advantageous for telecommunication applications [1], [2],[14]. In addition, a number of DFB fiber lasers can be configured in a parallel array to provide flexibility in pumping conditions and provide pump redundancy [2], [4]. Robust single polarization and narrow linewidth of DFB lasers are very desirable for sensor systems [5]–[7]. Alternatively, DFB lasers can be made to operate in stable dual polarization so that simultaneous measurements can be carried out [8]–[10]. In addition to the sensing and telecom applications, DFB fiber lasers suitable for high-power applications have been demonstrated [11].

An important feature of using DFB-Fiber Laser Sensors for various applications consists in the technology of analyzing the output. DFB-Fiber Laser Sensors are inherently fiber optic compatible, and very easy connected to other optoelectronic devices [3], [9], [21]-[24]. One of the most important aspect to be considered in designing DFB-Fiber Laser Sensors is the technology used for converting the useful information/signal from the optic domain (the photons being the carriers) to the electronic domain (the electrons being the carriers). The use of DFB-Fiber Laser as Sensors is based on observing the laser output variations versus the environment modifications. A "key" in designing properly DFB-Fiber Laser Sensors consists in a correct configuration of photo-detector circuit. DFB-Fiber Laser Sensors output variations can be caused by Er^{3+} doped fiber optic amplifier (EDFA) and/or Bragg Grating parameters modification. An important issue consists in designing the filters used to "cut off" noise of various types. It is important to understand what type of noise is filtered out, to understand its source. In this first part, some procedures considering the EDFA optoelectronic noise and used for designing such filters are presented.

II. Specification of active FBG sensor

Basically, the analyzed problem consists in evaluation of the noise magnitude into an active FBG output signal. Fig. 1 schematically presents the common experimental setup of this type of devices [10]-[20], [25].

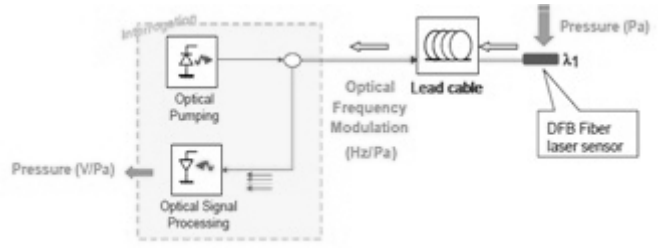

Fig. 1 Experimental setup allowing pumping and interrogation of the DFB-FL sensor. The "Optical Signal Processing" subsystem can be observed. Its main detection part consists of a photodiode reversed biased

Here can be observed the main parts of this setup, namely:

- the pump unit, usually a laser diode operated at 1480 nm

Manuscript received October 16, 2010. This work is a part of the research activities performed by Advanced Study Center–National Institute of Aerospace Research "Elie Carafoli", Bucharest, Romania and National Institute of R&D for Optoelectronics-INOE 2000, Bucharest, Romania in the frame of EU Research Program CLEANSKY-W.P. 1.3.7–Aerodynamic Sensors.

D. Savastru. is with the National Institute of R&D for Optoelectronics-INOE 2000, 409 Atomistilor str., P.O.B. MG-5, Magurele, Ilfov, Romania, tel:+40214575757, fax: +40214574522 (e-mail: dsavas@inoe.inoe.ro).

S. Miclos is with the National Institute R&D of Optoelectronics-INOE 2000, 409 Atomistilor str., P.O.B. MG-5, Magurele, Ilfov, Romania, tel:+40214575757, fax: +40214574522 (e-mail: miclos@inoe.inoe.ro).).

I. Lancranjan is with the Advanced Study Center–National Institute of Aerospace Research "Elie Carafoli", 220 Iuliu Maniu Blvd, Bucharest, Romania, tel: +40214340078, fax: +40214340082, (e-mail: ilancranjan@incas.ro).

or 980 nm pumping wavelength
- the lead cable, into which a WDM unit is inserted, WDM meaning wavelength demultiplexing, its role consisting into separation of pumping and laser signal,
- the "Optical Signal Processing" consisting of a reversed biased photodiode operated in charge generation regime.

One important investigated aeronautical DFB-FL and DBR-FL sensors application consists in determination of the transition zone (line) between laminar and turbulent air flow along the aircraft wing surface.

The laminar and turbulent boundary layers can be observed in Fig. 2.

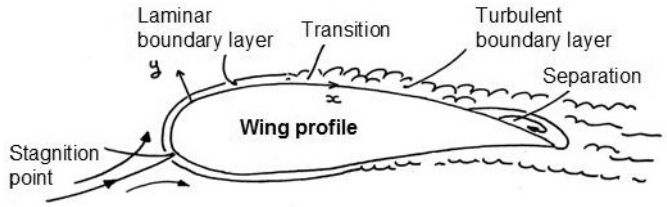

Fig. 2 Schematic representation of the main investigated aeronautical application of DFB-FL and DBR-FL

More insights about the investigated problem are schematically presented in Fig. 3.

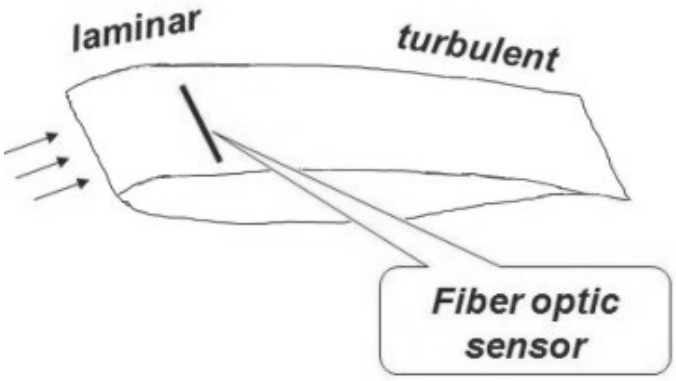

Fig. 3 Schematic representation with few relevant insights of the main investigated aeronautical application of active FBG sensor

The basic idea of this type of measurement is to evaluate the pressure variation in the two zones:

1. Laminar flow - relative constant value of air static pressure, low frequency (~ 100 Hz) and small amplitude ($\Delta P \sim 1$ Pa) pressure variations.
2. Turbulent flow - larger and nonstationary value of air static pressure, higher frequency (~ 10 kHz) and higher amplitude ($\Delta P \sim 10$ Pa) pressure variations.

Usually, the analyzed active FBG output signal appears as in Fig. 3. It can easily be observed that the linearity of active FBG sensor output signal and the magnitude of output noise are extremely important in order to obtain correct "responses" from the active FBG sensor.

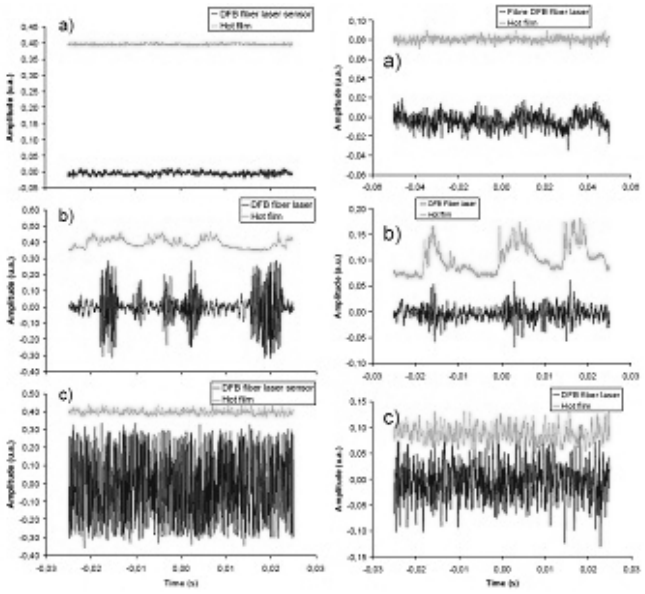

Fig. 4 Time evolution of the system output signal. Left : DFB-FL at the wing model surface. Right : DFB-FL buried at 200μm under the wing model surface. a) laminar regime, b) intermittent regime and c) turbulent regime. Dark curve : DFB fiber laser. Light curve : hot film [21].

III. Defining EDFA preamplifier and detector system

In Fig. 5 the schematic of the Erbium Doped Fiber Amplifier (EDFA), here used as a preamplifier of the laser sensor signal, and of the detector system is presented. The "border" between optical and electronic signal processing subsystems is marked explicitly. The PIN photodiode has the role of transforming the optical laser signal generated by the active FBG sensor into an electronic one [3], [5]-[11]. The characteristics of the photodiode are quite common – starting with the idea that a most general applicable analysis is of interest. It has to be underlined the important role of the 1 nm band-pass optical filter mounted at the PIN photodiode input port. The characteristics of the low-pass electronic mounted at PIN photodiode output gate depend on this optical filter.

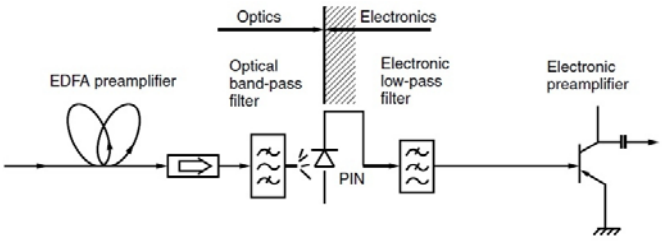

Fig. 5 General schematics of a laser signal receiver using EDFA as a preamplifier

In Fig. 6 the frequency ranges of an usual active FBG sensor are schematically presented. An important observation has to be made: the ASE noise frequency bandwidth, corresponding to the fluorescence emission FWHM can reach large val-

ues in case of band-pass optical filter absence. For example, in the case of using Erbium ions (Er^{3+}) as doping, having a 50 nm FWHM fluorescence band, the electronic low-pass filter have to be operated with a 5 THz frequency bandwidth [15], [17]-[20].

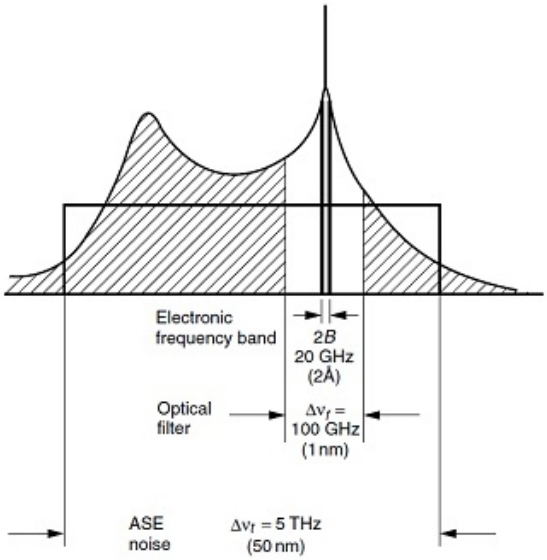

Fig. 6 Comparison of relative frequency ranges: ASE noise, optical filter, electronic frequency band

IV. EDFA THEORY

In Fig. 7 the principle of three-level optical amplifier mostly used in active FBG sensor is presented.

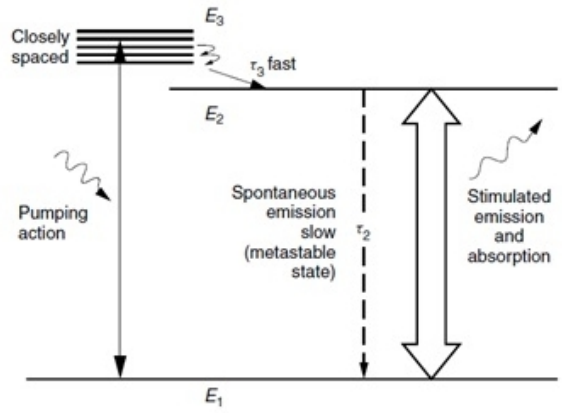

Fig. 7 Principle of three-level optical amplifier

Energy level E_3 is actually a bundle of many closely spaced energy levels, rather than one discrete level. When the pump light is turned on, upward transitions from E_1 to the E_3 band take place, provided the energies contained in the pump light match the E_1 to E_3 band transition. Almost immediately, downward transitions are initiated between the closely spaced E_3 levels, as well as from E_3 to the nearby level E_2. Because of the narrow spacing, the transitions between the E_3 levels are primarily associated with phonons and nonradiative transitions and occur very quickly over lifetimes of the order of femtoseconds to nanoseconds. The released energy is converted into crystal lattice vibrations or phonons with energy $h\nu_{phonon}$.

There is a large energy gap between E_2 and E_1, which means that photons are involved rather than phonons. The downward transition from E_2 to E_1 is responsible for the fluorescent glow. We are particularly interested in materials where E_2 is a metastable state, which means the downward transition from E_2 to E_1 occurs over a lifetime τ_2 of milliseconds to hours. Thus, $\tau_2 > \tau_3$ and the glow lasts a long time after the pump has been turned off.

The expression for the gain of an optical amplifier depends solely on the transitions between the two levels involved in the population inversion. This is true for both three-level and four-level models. In the preliminary discussion of fluorescence, the levels involved in the population inversion were distinctly well-defined levels. However, the description can easily be extended to a population inversion between two *bands* of energy levels. Whether the transitions involve molecules, atoms, ions, or electrons in the energy bands depends on the material. For the sake of generality, the term "carrier" is used to represent an atom, molecule, ion, or electron in a particular level.

Consider the two energy levels E_2 and E_1 shown in precedent Fig. 7, disregarding pump level E_3. Energy is released in a downward transition of a carrier, and energy is absorbed in an upward transition. Stimulated transitions, that is, transitions initiated by the presence of an external photon, take place in both directions. In stimulated absorption, the external photon is absorbed as the upward transition takes place, and in stimulated emission, the external photon causes the release of a photon of identical energy as the downward transition takes place. Spontaneous emission is the release of a photon in a downward transition that happens of its own accord, without any external influences. There is no such thing as spontaneous absorption, or a spontaneous upward transition. Since there is only one type of absorption, the qualifier "stimulated' is often dropped, and the process is simply called absorption [3], [8]-[13].

The dynamic evolution of an EDFA can be described by a system of rate equations, N_j being the population of level j:

$$\frac{dN_3}{dt} = W_p\left(N_1 - N_3\right) - \frac{N_3}{\tau_3} \tag{1}$$

$$\frac{dN_2}{dt} = \frac{N_3}{\tau_{32}} - \frac{N_2}{\tau_{21}} - W_s\left(N_2 - N_1\right) \tag{2}$$

$$\frac{dN_1}{dt} = -W_p\left(N_1 - N_3\right) + \frac{N_2}{\tau_{21}} + W_s\left(N_2 - N_1\right) \tag{3}$$

In (1)–(3), τ_{ij} is the lifetime of the i→j transition. Also, in this rate equations system there are introduced:
W_p - the stimulated transition probability between E_3 and E_1;
W_s - the stimulated transition probability between E_2 and E_1.
These parameters are defined as:

$$W_p(\nu_p) = \sigma_p \frac{I_p}{h\nu_p} \tag{4}$$

$$W_s(\nu_s) = \sigma_s \frac{I_s}{h\nu_s} \tag{5}$$

where I, σ and ν denote the pump or signal laser intensity, stimulated transition cross section and transition frequency. h is the Planck's constant.

The parameter of interest is the "gain factor" defined as:

$$\frac{N_2 - N_1}{N} = \frac{(1-\beta)W_p\tau_{21} - 1}{(1+\beta)W_p\tau_{21} + 2W_s\tau_{21} + 1} \tag{6}$$

N is the Er^{3+} concentration. β is the Boltzmann population ratio defined as:

$$\beta = \frac{N_3}{N_2} = e^{-\left(\frac{\Delta E}{kT}\right)} \tag{7}$$

In Fig. 8 the variation of EDFA gain versus pump rate is presented.

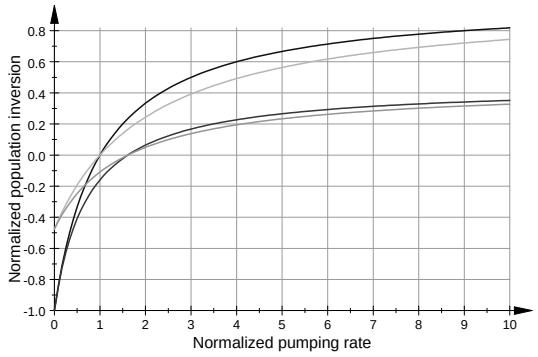

Fig. 8 Variation of population difference (gain) versus pumping rate in EDFA

V. Analysis of EDFA pumping

In the presented theoretical analysis the pumping wavelength plays an important role. In Fig. 9 a detailed schematic of EDFA pumping is presented. As it can be observed in Fig. 9, EDFA pumping is mostly performed by using two wavelengths: 980 nm and 1480 nm. For performing a proper analysis of pros and cons between these two wavelengths several criteria can be considered:

A - Boltzmann population ratio – $\beta_{1480} = 0.38$ while $\beta_{980} \sim 0$. This means an advantage for 980 nm pump wavelength.

B – The comparison can be done by using the relation

$$\left(\frac{N_2 - N_1}{N}\right)_{\max} = \frac{1-\beta}{1+\beta} \tag{8}$$

The net result is that, at the same pumping power, maximum gain for 1480 nm is 0.45 of that obtained by using 980 nm.

C - The amplified spontaneous emission (ASE) noise is proportional to n_{spon} defined as

$$n_{spon} = \frac{N_2}{N_2 - N_1} \tag{9}$$

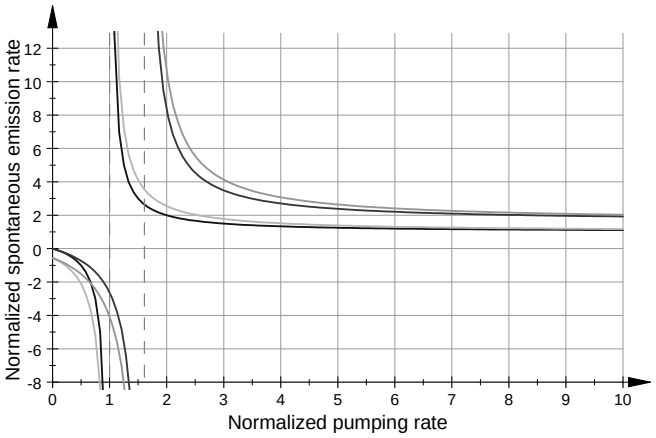

Fig. 9 Variation of normalized spontaneous emission versus pumping rate in EDFA

For the same pumping power, n_{spon} is 1.61 for 1480 nm versus the value for 980 nm. This means a greater noise for 1480 nm.

D - The threshold pump power defined as:

$$W_p^{th} = \frac{1}{1-\beta} \tag{10}$$

This means a 1.61 times higher threshold pump power for 1480 nm in comparison with 980 nm.

E - The saturation signal power intensity is defined as:

$$W_s^{sat} = \frac{1}{2}\left[(1+\beta)W_p + \frac{1}{\tau}\right] \tag{11}$$

It can be observed that, for the same pumping power, the saturation power is higher for 1480 nm pumping. This means extended sensor response linearity for the 1480 nm pumping.

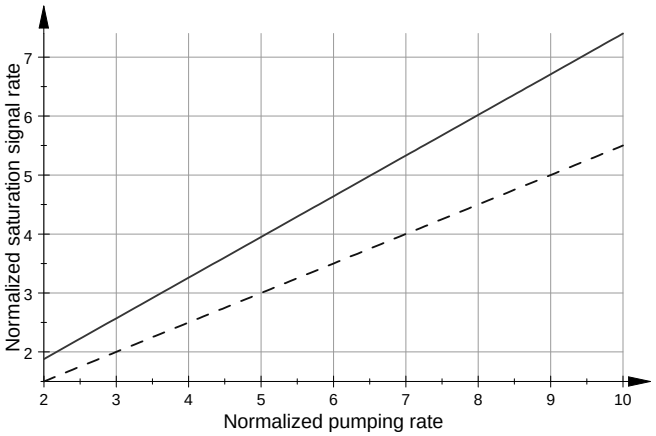

Fig. 10 Variation of normalized saturation power intensity versus pumping rate in EDFA. Dashed line represents 980 nm pumping while the solid line represents 1480 nm pumping

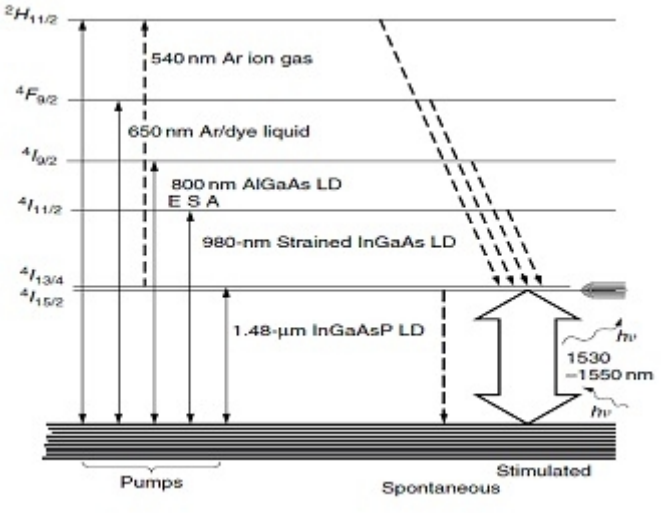

Fig. 11 The energy level diagram of Er^{3+}. There are indicated the types of lasers that may be used as the pump light

VI. EDFA PREAMPLIFIER AND DETECTOR OUTPUT NOISE ANALYSIS

The photodiode plays the role of the mixer between the signal and the ASE noise. The calculation method is the same as that of heterodyne detection but with the ASE noise as the local oscillator. In order to reduce the contribution of the ASE noise, a band-pass optical filter is installed at the end of the erbium-doped fiber, as shown in Fig. 5 [10],. If the ASE noise is uniformly spread over fluorescence bandwidth, the light output P from the EDFA through the optical filter with pass-band $\Delta\nu_f$ is defined as:

$$P = GP_S + GP_{ASE} \tag{12}$$

In (12) P_{ASE} represents the power of Amplified Spontaneous Emission and is defined as:

$$P_{ASE} = n_{spon} h\nu \Delta\nu_f \tag{13}$$

G represents the gain of EDFA. The output from the photodiode when the output P of (12) is fed to the photodiode will be calculated. The amplitude E_S and power GP_S of the light are related by:

$$GP_S = \frac{1}{2} \cdot \frac{E_S^2}{\eta_0} A_{photodiode} \tag{14}$$

In (14) η_0 is the intrinsic impedance of air but not that of the photodiode medium (the definition of the quantum efficiency has already accounted for the reflection at the air and photodiode boundary. The surface area of the photodiode is defined as $A_{photodiode}$. The amplitude of the input light signal into the photodiode $A_{photodiode}$ is defined by:

$$E_s = \sqrt{\frac{2\eta_0}{A_{photodiode}} GP_s} \tag{15}$$

If the assumption is made that the ASE noise spectrum can be represented as N discrete line spectra with equal powers of GP_{ASE}/N, as shown in Fig. 10, then the amplitude of each noise spectrum is:

$$E_n = \sqrt{\frac{2\eta_0}{A_{photodiode}} \cdot \frac{GP_{ASE}}{N}} \tag{16}$$

The photodiode plays the role of the mixer between the signal and the ASE noise. The calculation method is the same as that of heterodyne detection but with the ASE noise as the local oscillator. After some calculations, the sinusoidal wave expression for the instantaneous output electrical current $i(t)$ from a PIN photodiode is:

$$i(t) = \frac{\eta_e A_{photodiode}}{h\nu_S \eta_S} \cdot \left[E_S \cdot \cos(2\pi\nu_S t + \phi_S) + \sum_{n=1}^{N} E_n \cdot \cos(2\pi\nu_n t + \phi_n) \right]^2 \tag{17}$$

The first term is the signal and the second term is the sum of the N discrete ASE noise spectrum lines. The square operation creates a number of different beat frequencies that belong to the following three categories:

1. Signal current
2. Noise current due to the beats between the signal and the ASE noise whose beat frequencies fall within the electronic frequency bandwidth of the detector. This noise is called signal–spontaneous beat noise.
3. Noise current due to the beats among the line spectra of the ASE noise whose beat frequencies fall within the electronic frequency bandwidth of the detector. This noise is called spontaneous–spontaneous beat noise.

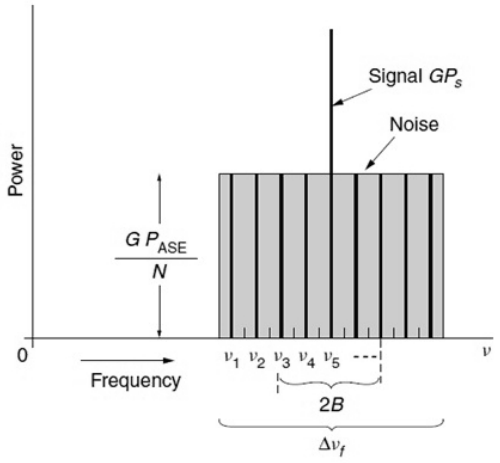

Fig. 12 Division of continuous ASE noise spectrum into discrete ASE noise line spectra

Concerning the signal current calculations, after some calculations which starts considering the photodiode signal current $i(t)$ defined as

$$i(t)=\frac{\eta e}{h\nu}\frac{A_{photodiode}}{\eta_0}E_s^2\cos^2(2\pi\nu_s t+\phi_s) \tag{18}$$

the following useful relations are obtained:

$$i(t)=\frac{\eta e}{h\nu}GP_s \tag{19}$$

and

$$S=\left(\frac{\eta e}{h\nu}GP_s\right)^2 R_L \tag{20}$$

In (20) S represents the electrical signal power while R_L is the load resistance of the photodiode.

Concerning the beats between the signal and the ASE noise issue, the signal-spontaneous beat noise current $i_{sig\text{-}spon}$ is the task to be accomplished. By treating each noise spectrum as a local oscillator, the output current due to the beat between the signal and only the n[th] noise spectrum is derived. The procedure starts by considering the relation

$$i_{sig-spon}(t)=2\frac{\eta e}{h\nu}\frac{A_{photodiode}}{\eta_0}E_sE_n \cdot\left[\sum_{n=1}^{N}\cos(2\pi\nu_s t+\phi_s)\cos(2\pi\nu_n t+\phi_n)\right] \tag{21}$$

The output current components from the photodiode are defined as:

$$i_{sig-spon}(t)=\frac{\eta e}{h\nu}\frac{A_{photodiode}}{\eta_0}E_sE_n \cdot\sum_{n=1}^{N}\cos[2\pi(\nu_s-\nu_n)t+(\phi_s-\phi_n)] \tag{22}$$

$i_{sig\text{-}spon}(t)$ has N discrete spectra that are the beats made by ν_n and ν_s, and they are the components that can pass through the electronic filter. N' - the number of frequency components of $i_{sig\text{-}spon}(t)$ in (21) and (22) that are within the frequency bandwidth $\Delta\nu_f$ and get through the electronic preamplifier is:

$$N'=N\frac{2B}{\Delta\nu_f} \tag{23}$$

Each spectrum has the same magnitude, and the total of the time averages of the beat current square is N' times and:

$$\left\langle i_{sig-spon}^2\right\rangle=4\left(\frac{\eta e}{h\nu}\right)^2 GP_s\cdot GP_{ASE}\frac{B}{\Delta\nu_f} \tag{24}$$

The current $\left\langle i_{sig-spon}^2\right\rangle$ is proportional to the product of the output signal power and the ASE noise.

Concerning the beats among the line spectra of the ASE noise spontaneous–spontaneous beat noise $i_{spon\text{-}spon}(t)$ is calculated. The noise current due to the j^{th} and k^{th} ASE noise line spectra are obtained from the square of the second term in (17), suppressing ϕ_n:

$$i_{spon-spon}(t)=\frac{\eta e}{h\nu}\frac{A_{photodiode}}{\eta_0} \cdot\left[\sum_j E_j\cos(2\pi\nu_j t)\right]\cdot\left[\sum_k E_k\cos(2\pi\nu_k t)\right] \tag{25}$$

This is the starting point for a similar procedure which leads, after a large amount of algebraic calculations to:

$$\left\langle i_{spon-spon}\right\rangle=\left(\frac{\eta e}{h\nu}GP_{ASE}\right)^2\cdot\left(2-\frac{B}{\Delta\nu_f}\right)\cdot\left(\frac{B}{\Delta\nu_f}\right) \tag{26}$$

where P_{ASE} is the ASE optical power and B is defined according to Fig. 12, being the bandwidth of the noise power subjected to the electronic preamplifier.

It has to be underlined that the two parameters are useful as "figure of merit" for characterizing a DFB-FL sensor:

- the signal generated photodiode current, I_s, defined as

$$I_s=\frac{\eta e}{h\nu}P_s \tag{27}$$

- the ASE generated photodiode current, I_{ASE}, defined as

$$I_{ASE}=\frac{\eta e}{h\nu}P_{ASE} \tag{28}$$

In (27) and (28), P_s and P_{ASE} are signal and ASE optical powers. It should be noted that I_s and I_{ASE} are the photocurrents from the photodiode with a unitary optical amplifier gain.

Based on the previously obtained results of the beat noises, the signal to noise ratio *S/N* of a receiver with an optical amplifier used as a preamplifier, as shown in Fig. 5 has to be found. Besides the above defined beat noises, the shot noise and thermal noise from the photodiode have to be included. The shot noise of the PIN diode is caused by the irregularity of the electron flow in the diode, and the shot noise power N_{shot} is defined as:

$$N_{shot}=2eI_tBR_L \tag{29}$$

where I_t is the total average current including the signal current, the ASE noise current and the dark current I_d of the PIN photodiode and R_L is the load resistance of the PIN diode.

The thermal noise is emitted from any medium that has nonzero Kelvin temperature. The thermal noise is given by:

$$N_{th} = \frac{4kTB}{R_L} \tag{30}$$

In k is the Boltzmann constant, and T is the absolute temperature in Kelvin.

The electrical S/N of the output from the PIN photodiode shown in Fig. 5 is defined as:

$$\frac{S}{N} = (GI_s)^2 / [4I_s I_{ASE} \frac{B}{\Delta\nu_f} + I_{ASE}^2 \left(2 - \frac{B}{\Delta\nu_f}\right) \frac{B}{\Delta\nu_f} + \frac{2eB}{G}\left(I_s + I_{ASE} + \frac{I_d}{G}\right) + \frac{4kTB}{G^2 R_L}] \tag{31}$$

As seen from (31), as G is increased, the contribution of the thermal noise is diminished the most, and then that of the shot noise, while the contributions of the signal–spontaneous noise and the spontaneous–spontaneous noise are left unchanged.

For large G, the S/N becomes:

$$\frac{S}{N} = \frac{I_s}{\left[4 + \frac{I_{ASE}}{I_s}\left(2 - \frac{B}{\Delta\nu_f}\right)\right] I_{ASE} \frac{B}{\Delta\nu_f}} \tag{32}$$

If the input photocurrent I_s is maintained much larger than I_{ASE} the ultimate S/N value of the receiver when the optical amplifier is used as an optical preamplifier is:

$$\frac{S}{N} = \frac{I_s}{4 \cdot I_{ASE} \frac{B}{\Delta\nu_f}} \tag{33}$$

Finally, for the noise ratio the following relation is obtained:

$$\frac{S}{N} = \frac{I_s}{\left[4 + \frac{n_{spon} h\nu \Delta\nu_f}{P_s}\left(2 - \frac{B}{\Delta\nu_f}\right)\right] n_{spon} h\nu B} \tag{34}$$

In terms of the light power (34) can be rewritten as:

$$\frac{S}{N} = \frac{P_s}{4 \cdot n_{spon} h\nu B} \tag{35}$$

It has to be noticed that the signal to noise ratio depends on quantity n_{spon} directly and by optical signal power. n_{spon} can be reduced by raising the light pumping level.

In order to define some useful quantifications concerning the above defined items, as an example, for a DFB-FL detector as defined in Fig. 5 with the wavelength bandwidth of the optical filter of 0.1 nm, with an n_{spon} of 2.25, at 1mW signal optical power, the ASE optical power has a value of 11.3 μW.

In Fig. 13 the variations of signal to noise ration as function of normalized pumping rate deduced for a DFB-FL sensor manufactured by using Er^{3+} doped optic fiber are presented. P_s is considered as a fixed parameter. In Table I the parameters of the analyzed DFB-FL sensor system are defined.

TABLE I
PARAMETERS OF THE DFB-FL SENSOR

Parameter	Value
Light signal power	$1 .. 25 \cdot 10^{-6}$ W
Wavelength	$1.55 \cdot 10^{-6}$ m
Optical filter bandwidth	$1.24 \cdot 10^{10}$ s^{-1}
Electrical signal bandwidth	$6.2 \cdot 10^{9}$ s^{-1}
Dark current of the PIN diode	0
Load impedance to the PIN diode	50 Ω
Room temperature	300 K

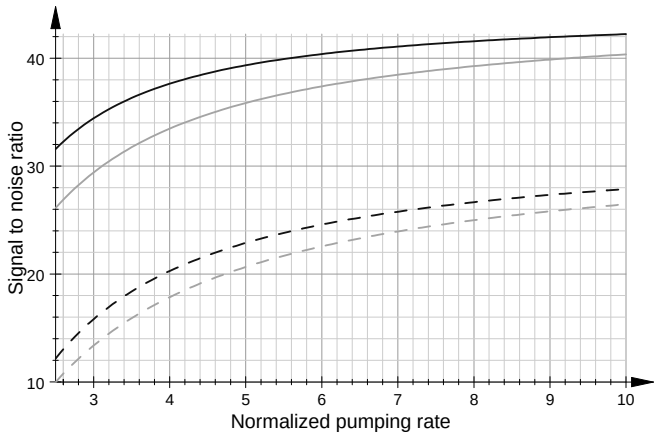

Fig. 13 Signal to noise ratio vs. normalized pumping rate. Solid lines correspond to the 980 nm pumping while dashed lines correspond to the 1480 nm pumping

It has to be noticed that by performing complicated calculations, a design procedure for creating active FBG sensors is developed allowing an advertised choice of the pumping wavelength and power.

VII. CONCLUSION-RESULTS

The main result of the presented theoretical analysis consists in the following conclusions, regarding the aeronautical application of interest:

- Depending on the magnitude of environment parameters to be observed, the pumping wavelength is chosen, in order to define a domain of linear response of the sensor covering the maximum value of the input environment parameter.
  In this sense the results presented in Fig. 4 are more than acceptable.
- Depending on the magnitude of environment parameters to be observed, the pumping power level is set at an optimum such that noise due mainly to ASE is kept at an acceptable level.
  In this sense the results presented in Fig. 4 are acceptable.
- An important factor of the performed analysis is the "time response" of the active FBG, meaning if there are disturbances of the sensor output signal regarding the time scale of environment parameters variations.

In this sense, the results presented in Fig. 4 illustrates that the active FBG acts like a high fidelity recorder, its characteristic times being much shorter than the observed pressure variations.

The presented preliminary theoretical analysis will be further developed pointing for various new aeronautic applications.

REFERENCES

[1] T. Miyazazaki, K. Inagaki, Y. Karasawa, and M. Yoshida, "Nd-doped double-clad fiber amplifier at 1.06 mm," *J. Lightwave Technol.* **16**(4), 562–566 (1998).

[2] K. Isshiki, H. Sasamori, H. Watanabe, K. Kasahara and K. Ito, "A 980-nm band laser diode pump source with a detuned wavelength of 1000 nm for praseodymium doped fiber amplifiers," *J. Lightwave Technol.* **16**(3), 401–404 (1998).

[3] A. Yariv, *Optical Electronics*, 4th ed., Saunders, Philadelphia, PA, 1991.

[4] E. Desurvire, *Erbium-Doped Fiber Amplifiers: Principles and Applications*, Wiley, New York, 1994.

[5] W. J. Miniscalco, "Erbium-doped glasses for fiber amplifiers at 1500 nm," *J. Lightwave Technol.* **9**(2), 234–250 (1991).

[6] A. E. Siegman, *Lasers*, University Science Books, Mill Valley, CA, 1986.

[7] K. Nakagawa, S. Nishi, K. Aida, and E. Yoneda, "Trunk and distribution network application of erbium-doped fiber amplifier," *J. Lightwave Technol.* **9**(2), 198–208 (1991).

[8] E. Desurvire, "Analysis of transient gain saturation and recovery in erbium-doped fiber amplifiers," *IEEE Photonics Technol. Lett.* **1**(8), 196–199 (1989).

[9] S. Mookherjea, "Remotely pumped optical distribution networks: A distributed amplifier model," *J. Lightwave Technol.* **19**(7), 926–932 (2001).

[10] Y. Hirano, Y. Shoji, K. Kasahara, M. Yoshida, T. Araki, and Y. Hisada, "Multiwatt operation of square-shaped double-clad Nd-doped fiber amplifier," *Conference on Lasers and Electro-Optics (CLEO'98)*, pp. 427–428, 1998.

[11] P. Glas, M. Naumann, A. Schirrmacher, and Th. Pertsch, "A CW diode-pumped single silica fiber comprising 40 cores used as active elements for a high power fiber laser at lD 1050 nm," *Conference on Lasers and Electro-Optics (CLEO'98)*, pp. 113–114, 1998.

[12] S. Wen and S. Chi, "Characteristics of the gain and signal-to-noise ratio of a distributed erbium-doped fiber amplifier," *J. Lightwave Technol.* **10**(12), 1869–1878 (1992).

[13] Y. H. Cheng, "Optimal design for direct-detection system with optical amplifiers and dispersion compensations," *J. Lightwave Technol.* **11**(9), 1495–1499 (1993).

[14] S. Ryu, *Coherent Lightwave Communication Systems*, Artech House, Boston, (1995).

[15] V. Arya and I. Jacobs, "Optical preamplifier receiver for spectrum-sliced WDM," *J. Lightwave Technol.* **15**(4), 576–583 (1997).

[16] N. S. Sergano and C. R. Davidson, "Wavelength division multiplexing in long-haul transmission systems," *J. Lightwave Technol.* **14**(6) 1299–1308 (1996).

[17] S. Sudo, *Optical Fiber Amplifiers: Materials, Devices and Applications*, Artech House, Boston, 1997.

[18] M. J. Yadlowsky, E. M. Deliso, and V. L. Da Silva, "Optical fibers and amplifiers for WDM systems," *Proc. IEEE* **85**(11), 1765–1779 (1997).

[19] P. Laperle, R. Vall´ee, and A. Chandonnet, "Stable blue emission from a 2500 ppm thulium-doped ZBLAN fiber laser," *Conference on Lasers and Electro-Optics (CLEO'98)*, pp. 77–78, 1998.

[20] W. Lenth and R. M. Macfarlane, "Upconversion lasers," *Opt. Photonics News* **3**(3), 8–15 (1992).

[21] Ismail Kucuk, Ibrahim Sadek, Yalcin Yilmaz and Salma Islam "Optimal Vibration Control of Beam Using Piezoceramic Actuators and Sensors," Proceedings of LATEST TRENDS on APPLIED MATHEMATICS, SIMULATION, MODELLING (ASM'10), Corfu Island, Greece, July 22-25, 2010, pp.57-60

[22] K. Hasikin, N. Soin, F. Ibrahim "Modeling an Optical Diaphragm for Human Pulse Pressure Detection," Proceedings of the 8th WSEAS International Conference on Microelectronics, Nanoelectronics, Optoelectronics (MINO '09), Istanbul, Turkey, May 30 - June 1, 2009, pp.97-102

[23] Farzin Emami and Amir H. Jafari "Nonlinear Fiber Bragg Gratings," Proceedings of the 8th WSEAS International Conference on Microelectronics, Nanoelectronics, Optoelectronics (MINO '09), Istanbul, Turkey, May 30 - June 1, 2009, pp.118-123

[24] Filip Dvořak, Jan Maschke and Čestmir Vlček "Fiber sensor of temperature field disturbance," Proceedings of LATEST TRENDS on CIRCUITS, SYSTEMS and SIGNALS (CSS'10), Corfu Island, Greece, July 22-25, 2010, pp.134-140

[25] S. Molin, D. Dolfi, M. Doisy, A. Seraudie, D. Arnal, E. Coustols "Experimental study for the detection of the "laminar/turbulent" aerodynamic transition on a wing aircraft, using fiber optic sensors" – to be published in the frame of EU Research Program CLEANSKY –Working Package 1.3.7- Aerodynamic Sensors